Release of Different Cell Mediators During Retinal Pigment Epithelium Regeneration Following Selective Retina Therapy

Elisabeth Richert,[1] Stefan Koinzer,[1] Jan Tode,[1] Kerstin Schlott,[2] Ralf Brinkmann,[2] Jost Hillenkamp,[1,3] Alexa Klettner,[1] and Johann Roider[1]

[1]Department of Ophthalmology, Christian Albrechts University Kiel, Kiel, Germany
[2]Medical Laser Center Lübeck, Lübeck, Germany
[3]Department of Ophthalmology, University of Würzburg, Würzburg, Germany

Purpose. To investigate the effect of selective retina therapy (SRT) on the release of AMD relevant cell mediators, such as matrix metalloproteinases (MMPs), VEGF, and pigment epithelium derived factor (PEDF) using different laser spot sizes and densities.

Methods. Porcine RPE choroid explants were treated with a pulsed 532 nm Nd:YAG laser using (1) large spot sizes, (2) small spot sizes with a high density (hd) treatment, and (3) small spot sizes with a low density (ld) treatment. Explants were cultivated in modified Ussing chambers. RPE regeneration and RPE cell death were investigated by calcein AM staining and immunofluorescence. The MMP release was examined via zymography and immunofluorescence. VEGF and PEDF secretion was analyzed by ELISA.

Results. During pigment epithelium regeneration (PER), mitosis and RPE cell migration were observed. Four days after SRT (large spot size) the content of active MMP2 increased significantly ($P < 0.01$). Hd treatment with small spot sizes resulted also in an increase of active MMP2 ($P < 0.05$). In immunofluorescence explants showed a localized expression of MMP2 within the healing lesions after irradiation. The PEDF level increased significantly ($P = 0.01$) after SRT with large spot sizes. VEGF secretion decreased significantly ($P < 0.05$) following SRT with large spot sizes and with hd treatment of small spot sizes.

Conclusions. SRT induces a cytokine profile, which may improve the flux across Bruch's membrane, slows down progression of early AMD by RPE regeneration, and inhibits the formation of choroidal neovascularization. The cytokine release depends on the size and density of applied laser spots.

Keywords: age related macular degeneration, matrix metalloproteases, pigment epithelium derived factor, retinal pigment epithelium, selective retina therapy, vascular endothelial growth factor

AMD is the main cause for legal blindness of the elderly in Western civilizations.[1] The slowly progressing dry form of AMD is characterized by the presence of drusen and macular pigment alterations. Dry AMD may either progress into the exudative form or lead to macular atrophy, in which the RPE degenerates, followed by a loss of photoreceptors, resulting in vision deterioration.[2–4] An adequate pathomechanism driven therapy for the dry form of AMD is not available at present.[5] One factor in the complex pathophysiology of AMD is the age dependent alteration of Bruch's membrane (BrM), which is associated with a reduced ability to exchange nutrients and waste products between retina and choroid.[6–8] These alter ations are created by a disturbed balance in degradation and synthesis of BrM matrix. In advanced stages, the BrM is thickened and the reduced exchange leads to an undersupply of the neuroretina, which promotes AMD progression.[9–12]

The degradation and rebuilding pathway of BrM is mediated by the family of matrix metalloproteinases (MMPs) and their antagonists, the tissue inhibitors of metalloproteinases (TIMPs).[13] In particular, MMPs 1, 2, 3, and 9 and TIMPs 1, 2,

and 3 are part of BrM and secreted by the RPE and choroidal endothelial cells.[14–17] Contents of proforms of MMP2 and MMP9 have been shown to increase with age, whereas active forms are reduced or undetectable, which could explain the limited degradation ability of extracellular matrix (ECM) in aged eyes.[15,18] The stimulation of the MMP pathway could be a therapeutic option to reduce a thickened BrM, as seen in AMD, and thereby improve the flux across the BrM to slow down or prevent the progression of early AMD.[19]

Another important factor in AMD pathology is the balance between the expression of proangiogenic and antiangiogenic cell mediators.[20] The proangiogenic VEGF is the major factor in the development of choroidal neovascularizations (CNV) in wet form of AMD[21] and mainly secreted by the RPE.[22]

The pigment epithelium derived factor (PEDF), a powerful inhibitor of angiogenesis, is strongly associated with VEGF regulation, development, and survival of photoreceptors, as well as neuroprotection.[23–26] Former AMD related studies have shown that PEDF prevents formation of new blood vessels in murine models with laser induced CNV.[27] Creation of a protein
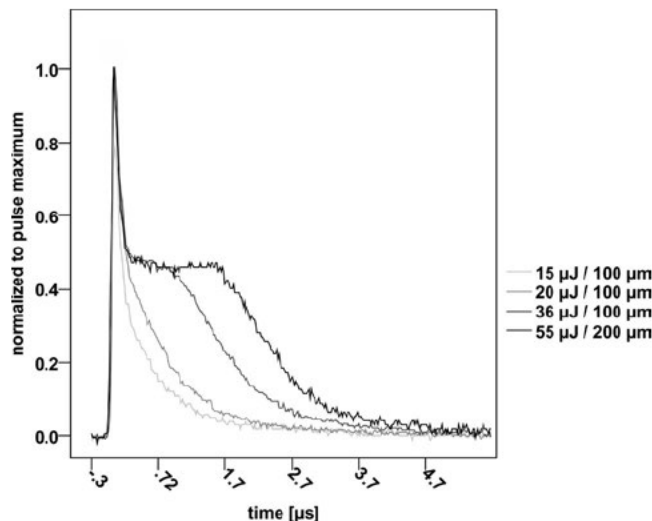
Figure 1. Duration of laser pulses with different energies. Two different forms of laser pulses arose depending on laser energies. An energy of 15 µJ resulted in pulses with a pulse duration of 1.04 µs. Pulse duration of pulses with 20 µJ was 1.36 µs. Above an energy level of 30 µJ, pulses with a "shoulder" arose and pulse duration extended. An energy of 36 µJ resulted in pulses with a pulse duration of 2.40 µs, while pulse duration of pulses with an energy of 55 µJ was 3.04 µs.

profile with nonneovascular properties would be a therapeutic option for prevention of AMD progression into wet AMD.

Early laser studies have shown that conventional photocoagulation is effective in the resolution of soft drusen, which are characteristic for dry AMD.[28,29] The observed drusen regression may be correlated with activation of ECM degrading cytokines, such as MMPs, secreted by RPE cells during regeneration. However, the use of conventional laser systems results in thermal defects of the neuroretina followed by scotoma.[30] Therefore, conventional laser lesions were applied in the periphery to avoid central macular damage.[29,31] The AMD pathology is limited to the macular region, and therefore it seems to be plausible that studies reported a limited or inexistent vision gain in patients treated with conventional photocoagulation in the periphery.[32,33]

The selective retina therapy (SRT) is a laser based method, which selectively targets the RPE but avoids thermal damage of the neurosensory retina or BrM.[34–37] SRT treatment causes a rapid formation of microbubbles around melanosomes, which results in selective disruption of RPE cell membranes.[38] RPE regeneration follows by migrating and proliferating of RPE cells, which cover the SRT induced lesion. In vitro studies showed the influence of SRT on the release of different cell mediators (e.g., activated MMPs).[39,40] Former clinical pilot studies showed positive effects of SRT in cases of drusen maculopathy, diabetic maculopathy, and central serous chorioretinopathy,[41–44] which support the concept of rejuvenation of RPE BrM complex by SRT.

We aim to generate a cytokine profile that might revitalize the RPE BrM complex to prevent the development or progression of early AMD using SRT. Therefore, we investigate the effect of SRT on the release of different AMD relevant cell mediators during pigment epithelium regeneration (PER). Furthermore, we report the initial results of the difference in cytokine release using SRT with varying spot sizes and densities. SRT treatment with smaller spots would allow a precise treatment even in the vision determining region, the fovea.

MATERIALS AND METHODS

Preparation of RPE–Choroid Explants

RPE choroid explants, consisting of RPE, BrM, and choroid, were prepared as previously described.[39] In brief, fresh porcine eyes were opened and anterior segment and vitreous were removed. Eyes were incised on one side and RPE, BrM, and choroid were carefully removed from the sclera. The retina was removed and explants were fixed within two polyacetal fixation rings (inner diameter 7 mm, height 1 mm). The area of the RPE layer was always the same and constantly filled with RPE cells so ensure the integrity of organ cultures. In cases where RPE choroidal tissues overlapped the outer margin of the rings, these areas were removed with a scalpel, to minimize artifacts of unspecific secondary stress response of RPE cells.

Explants were transferred into 12 well culture plates with 1.5 mL warm culture medium containing equal amounts of Dulbecco's modified Eagle's medium (glucose 4.5 g/L, L Glutamine, w/o Phenol Red; PAA, Pasching, Austria) and Ham's F12 medium (PAA) supplemented with 1% penicillin/streptomycin (Biochrom, Berlin, Germany), 5% to 10% fetal calf serum (Linaris, Wertheim Bettingen, Germany), 100 µM taurine (Sigma, Steinheim, Germany), and 2 mM calcium (Sigma).

Threshold Titration of Laser-Induced RPE Cell Death

We used a prototype Nd:YAG laser (Carl Zeiss Meditec AG, Jena, Germany) with 532 nm wavelength, which is transmitted by a multimode optical fiber with a square core profile of 70 µm, 100 Hz of repetition rate, and 30 pulses per irradiation, connected with a slit lamp. Depending on the used pulse energy, two forms of pulses arose (Fig. 1).

The spot size on the explants was chosen to 100 or 200 µm by magnification. For laser irradiation, a 12 well plate containing RPE choroid explants was placed on a metal board on the chin rest of the slit lamp. RPE integrity was analyzed via slit lamp examination with a mirror affixed to the slit lamp. Explants were treated with laser radiant exposure between 120 and 220 mJ/cm^2 per pulse. Irradiation levels were tested with Thermal Power Sensor S302C (Thorlabs, Lübeck, Germany). Four trial lesions with directly visible RPE destruction were set in a square formation to determine the titration region. Three test lesions per irradiance level were set within the titration region. Threshold titration of laser induced cell death was investigated by calcein AM vitality staining after a 24 hour incubation. For calcein staining, explants were incubated with calcein AM (4 µg/mL; AnaSpec, San Jose, CA, USA) for 45 minutes and washed twice with PBS (Serva, Heidelberg, Germany). RPE cell death was investigated by fluorescence microscopy (Axiovert 100; Carl Zeiss, Jena, Germany) with $\lambda ex/\lambda em = 497/517$ nm. Images were taken by Axio cam (MRc5; Carl Zeiss). Areas of cell death were analyzed with a semiautomatic program in AxioVision V 4.7.2.0 (Carl Zeiss) and calculated as percentage of the irradiated area. Irradiated areas that contained more than 50% dead cells were defined as lesions above the threshold and were used for further experiments.

RPE Regeneration and Examination of Cell Size and Number

RPE regeneration to laser induced wounds was examined after two different time intervals (1 and 4 days after SRT laser irradiation) via calcein staining. Images were taken as described above. The cell number was determined within the maximally irradiated area (0.04 mm^2) using SRT with 200

μm spot size. Cells were counted with a semiautomatic program in AxioVision in defined areas of RPE.

Scanning Electron Microscopy

The organ cultures were treated with pulsed laser irradiations (100 μm spot size, 200 mJ/cm^2, 100 Hz of repetition rate, and 30 pulses per irradiation) in a square formation of four trial lesions as described above. The samples were cultivated for 6 hours in cell culture medium at 37°C. After cultivation the samples were stored in 2.5% Glutaraldehyde until further use. The explants were rinsed in 0.1 M phosphate buffer and treated with 2% osmium. Afterward, they were dehydrated in increasing concentrations of ethanol, dried by a critical point dryer, and sputtered with gold targets. Samples were investigated using a XL20 scanning electron microscope (Philips, Eindhoven, the Netherlands).

Laser Treatment and Cultivation of RPE–Choroid Preparations in Modified Ussing Chambers

Cultivation of RPE choroid explants in modified Ussing Chambers allowed a differentiation of basal (choroid facing) and apical (RPE facing) protein secretion.[39] Tightness of the system was tested after 3 days of culture in Ussing chambers using Brilliant blue G (Brilliant peel; Fluoron, Ulm, Germany) in basal compartment by measured of a possible amount in the opposing compartment by photometry at 584 nm (Spectronic Genesys 10 Bio; Thermo Fisher Scientific, Waltham, MA, USA). A passage of Brilliant blue from basal to apical compartment was not observed (data not shown).

We prepared two organ culture rings from one eye and compared the release of different cell mediators of every SRT treated organ culture with an untreated control culture, prepared from the same eye.

Explants were treated with a radiant exposure of 200 mJ/cm^2 per pulse for small 100 μm spots and 140 mJ/cm^2 per pulse for larger 200 μm spots. Three different types of treatments were applied: large spot size (200 μm, 70 spots), small spot size (100 μm) with a low number of spots (low density; ld, ~280 spots), and small spot size (100 μm) with a high number of spots (high density; hd, ~550 spots). The total area of cell destruction depends on spot size and density. In cases of SRT with 200 μm spot size, the maximal destroyed area was 7% of the whole explant. After SRT with 100 μm in a hd treatment the maximal destroyed area was 14% and 7% in ld treatment.

Preparations were inserted in modified Ussing Chambers and each compartment was filled with 1.1 mL medium and incubated at 37°C and 5% CO_2. Culture medium was replaced every 24 hours. The basal supernatants were collected, centrifuged, and stored at 20°C.

Detection of Matrix Metalloproteases Via Zymography

Twenty microliters of zymogram sample buffer (Bio Rad, München, Germany) were added to 10 μL of control medium, basal supernatants of treated explants, or untreated controls, respectively, and was loaded onto 10% zymogram ready gel (Bio Rad). Proteinases were separated via electrophoresis (20 mA, 150 V for 30 minutes, and 50 mA, 200 V for 40 minutes). Gels were washed in aqua dest and incubated in renaturation buffer (2 × 30 minutes; Bio Rad) and developing buffer (Bio Rad) at 37°C (~18 hours). Gels were stained with Commassie Blue (Bio Rad) for 3 hours and destained with destaining solution (Bio Rad) for 1 hour. Densitometric MMP evaluation was performed with MF ChemiBis 1.6 Imager (Biotek, Jahns-

dorf, Germany) and 1D analysis (Total Lab TL100; Biosystematica, Mountain Hall, Great Britain). Contents of MMPs were depicted as x fold of untreated control after subtraction of medium control.

Detection of MMP2 and Ki-67 by Immunofluorescence

Expression of MMP2 and Ki 67 were observed by immuno fluorescence. Explants were fixed with 4% paraformaldehyde (PFA; Carl Roth, Karlsruhe, Germany) on ice, incubated in PFA:PEM (1:1) for 5 minutes and PFA:Borat (1:1) for 10 minutes, and washed with PBS. Afterward, explants were treated with Triton X 100 (5 minutes), $NaBH_4$ (10 minutes), and washed in PBS twice following 1 hour in Immunoblock (Carl Roth). Staining was performed with primary antibodies for MMP 2 (Santa Cruz Biotechnology, Inc., Heidelberg, Germany) and Ki 67 (Abcam, Cambridge, United Kingdom) at 4°C over night. Explants were washed with PBS three times and stained with Phalloidin Atto 488 (Sigma), Hoechst (Sigma), and Alexa fluor 647 donkey α goat (Invitrogen, Darmstadt, Germany), following wash steps with PBS and aqua dest. Explants were removed from rings and covered with Fluoromount G (EBioScience, San Diego, CA, USA) under cover slips. Fluorescence microscopy was performed at Axio Imager microscope 2 (Carl Zeiss); images were taken with Axio cam MRc5 and processed with Zen 2012 (Carl Zeiss).

Detection of VEGF$_{165}$ and PEDF via ELISA

Secretion of VEGF$_{165}$ and PEDF in culture medium of basal Ussing compartment was analyzed by a human specific VEGF$_{165}$ ELISA (R&D Systems, Minneapolis, MN, USA), which has the ability to detect porcine VEGF[45] and a porcine specific PEDF ELISA (Novateinbio, Woburn, MA, USA), respectively.

Statistics

Each experiment was performed with a minimum of three times and statistical analyses were conducted with Student's t test or ANOVA, respectively, using SPSS version 23 (IBM Corp., Armonk, NY, USA). A value of $P < 0.05$ was considered significant.

RESULTS

RPE Threshold Titration After SRT Treatment

For a spot size of 100 μm, laser radiant exposures of 150 mJ/cm^2 did not result in cell death. Laser radiant exposures of 180 mJ/cm^2 led to lesions above the threshold in 57% of the applied laser spots, whereas 200 mJ/cm^2 resulted in lesions above the threshold in 87%. An irradiation of 220 mJ/cm^2 produced 100% lesions above the threshold.

For a laser spot size of 200 μm, radiant exposures of 120 mJ/cm^2 did not result in cell death. Irradiation with 140 mJ/cm^2 resulted in lesions above the threshold in 61% of the applied laser spots. Of the applied spots, 180 mJ/cm^2 led to lesions above the threshold in 100%.

The aim of the PER was to irradiate the cells with energies that produce lesions above the threshold in more than 60% but less than 100% of applied laser spots. For this reason, we used radiant exposures of 200 mJ/cm^2 for a spot size of 100 μm and 140 mJ/cm^2 for a spot size of 200 μm in all cultivation experiments.
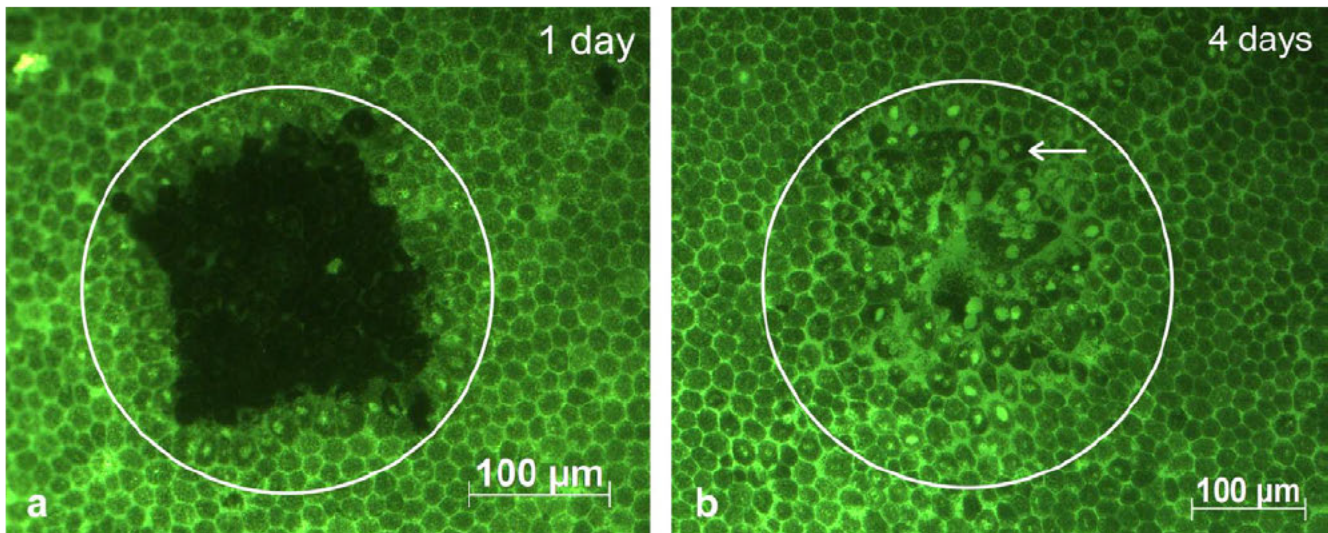
FIGURE 2. Different stages of RPE regeneration after SRT irradiation with 200 μm spot size. One day after irradiation with a radiant exposure, which resulted in lesions above the threshold of cell death (200 μm spot size, 140 mJ/cm² per pulse) calcein vitality staining showed the full effect of SRT (a). Four days after SRT, irregular shaped cells with conspicuous nuclei covered the laser induced RPE wound. Some of these enlarged cells showed two nuclei (*arrow*), which suggest mitosis (b).

RPE Cell Morphology, Cell Size, and Cell Proliferation During PER

As a consequence of SRT, the RPE cells in irradiated areas were destroyed. RPE choroid explants showed vitality and recovery of laser lesions under nutritional conditions. After 24 hours, the full effect of SRT could be observed in the RPE (Fig. 2a). During regeneration the cells at the rim of the SRT induced RPE lesion began to cover the wound. These cells were irregularly shaped with conspicuous nuclei. Four days after SRT the wound was completely covered (Fig. 2b). The size of cells, which covered the wound increased ($P < 0.01$) at day 4 in comparison to untreated RPE cells (Fig. 3a). Of lesion covering cells, 5% to 14% showed two nuclei.

During PER, the cell number within the destroyed area increased continuously and was significantly different between the different time points of examination ($P < 0.01$). The RPE cell number of untreated areas was determined as baseline per spot size. Two days after SRT, 8% RPE cells related to RPE baseline were present in the laser treated area. After 3 days of regeneration, cell count analysis showed an increase of cells in irradiated areas up to 37% and 53% after 4 days compared with untreated RPE (Fig. 3b).
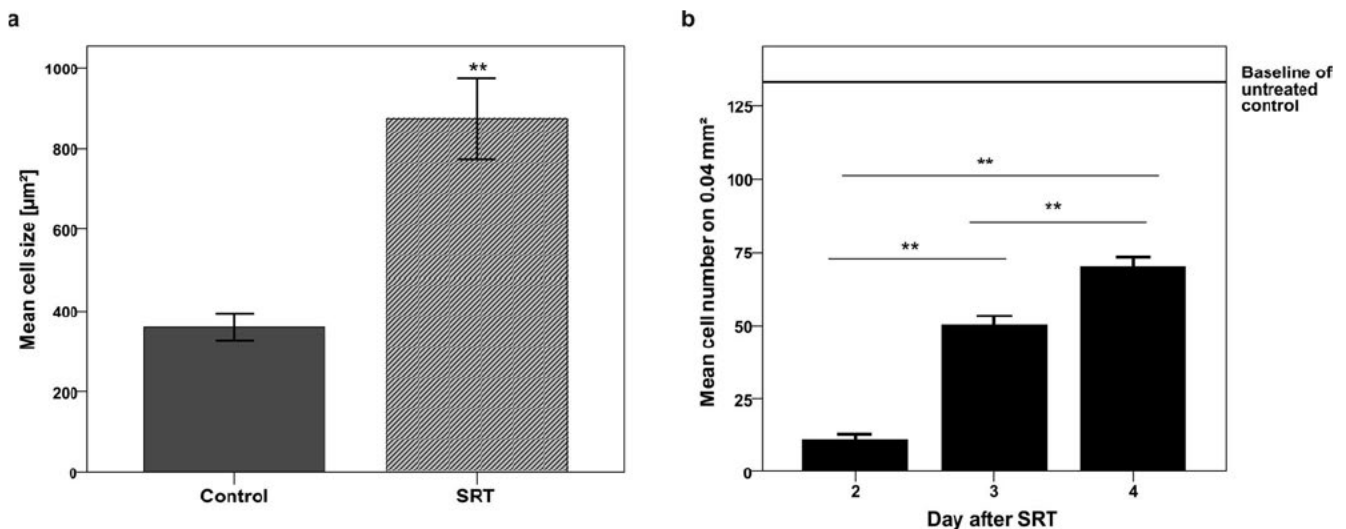

FIGURE 3. Variation of cell size and cell number during RPE regeneration. Four days after SRT the mean cell size (874 μm ± SEM 98) within the healing SRT area increased up to 2.4 fold in comparison to untreated RPE cells (360 μm ± SEM 32) (a). The number of cells increased during regeneration at day 2 to 4 within the treated SRT area. Two days after SRT, 8% RPE cells (11 cells ± SEM 2) related to baseline (133 cells ± SEM 6) were present in the irradiated area. Three days after SRT the cell number increased up to 37% (50 cells ± SEM 3). Four days after SRT cell number in irradiated area increased up to 53% (70 cells ± SEM 3) related to baseline of untreated control (b). This suggests both, cell migration and proliferation of cells, which covered the SRT lesion. (**$P < 0.01$).
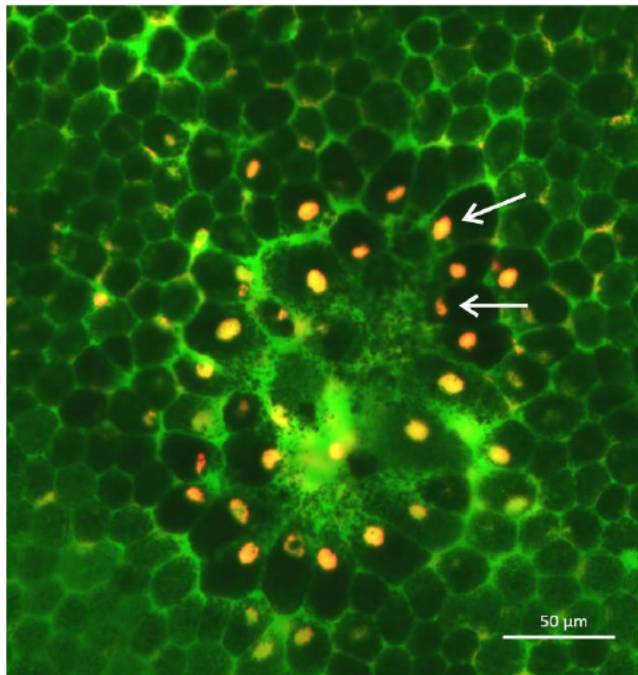
FIGURE 4. Immunofluorescence staining of mitosis marker Ki 67 at RPE choroid explants 3 days after SRT. In immunofluorescence we observed localized positive signals (*arrows*) of mitosis marker Ki 67 (*orange*) in cells surrounding the SRT area (200 µm spot size, 140 mJ/cm^2 per pulse), indicating RPE regeneration. Untreated RPE showed no signal for Ki 67.

In addition, cells surrounding the SRT area were positive for the cell proliferation marker Ki 67, whereas untreated RPE showed no signal for Ki 67 (Fig. 4).

Integrity of RPE–BrM Complex After SRT

We investigated the effect of SRT on RPE cells and underlying extracellular matrix by scanning electron microscopy. We observed the discrete selective destruction of RPE after 6 hours without damage of underlying RPE basal lamina and extracellular matrix (Fig. 5a). Damage of cell membranes might be the effect of SRT induced microbubbles after SRT as described by others[35,36,38,46] (Fig. 5b). Apical microvilli are absent after SRT compared with untreated cells (Fig. 5c).
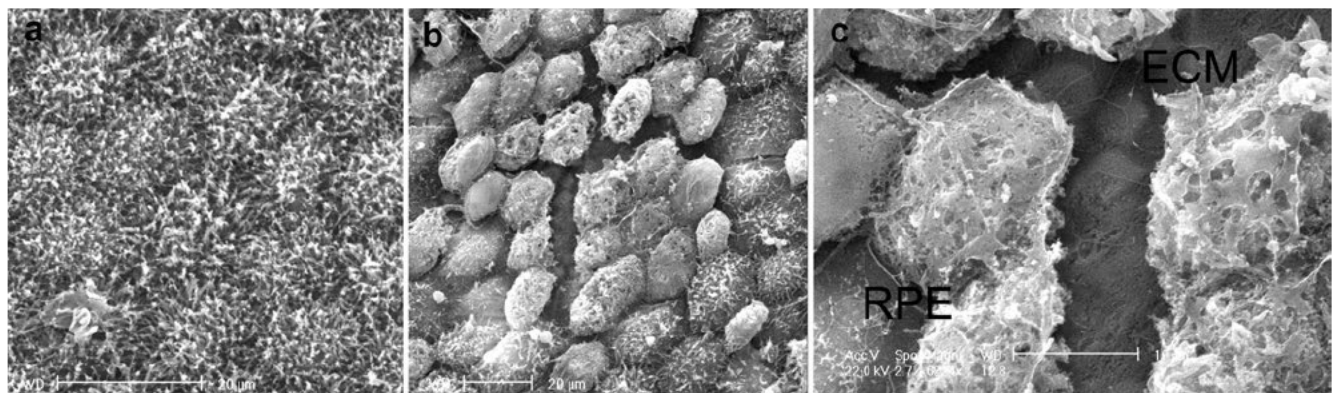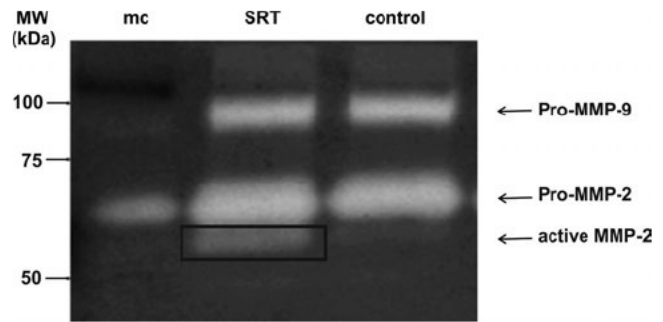

FIGURE 6. Representative zymogram displaying basolateral MMP release of irradiated and untreated organ cultures. Pro MMP9 (98 kDa), pro MMP2 (65 kDa), and active MMP2 (56 kDa) were detectable in culture medium of basal compartments of modified Ussing chambers at day 4 of cultivation. Active MMP 9 was not detectable. In medium control (mc) some pro MMP2 was detectable because of the background activity of 5% fetal calf serum. The zymogram is showing the moderate increase of pro MMP9 and pro MMP2 as well as the significant increase of active MMP2 in SRT treated explants (200 µm spot size) related to control.

Release of MMPs and Expression of MMP2 After SRT

SRT spots of 200 µm size are known to induce MMP secretion and activation.[39] To compare the effect of different spot sizes and densities on MMP release, we analyzed the basolateral MMP secretion. A representative zymogram, which is showing the release of different MMPs in irradiated and untreated explants, is shown in Figure 6. Pro MMP9 (98 kDa) was always detectable in basal compartments of modified Ussing chambers, while active MMP9 (88 kDa) could not be found in any sample tested. Pro MMP 2 (65 kDa) and active MMP2 (56 kDa) were always detectable in basal compartments at day 4.

MMP Secretion After SRT

At day 4 of cultivation the content of MMPs in the basal culture medium of the explants, which were irradiated with a ld of small 100 µm spots, was not altered. In contrast, in the hd group with 100 µm spots and an increased cumulative treated area compared with the other groups, we observed a moderate but significant increase ($P < 0.05$) of active MMP2 compared with control, while pro MMP9 and pro MMP2 were not altered. Four days after SRT with 200 µm spots, pro MMP9 and pro

FIGURE 5. Scanning laser microscopy of a porcine RPE choroid explant 6 hours after SRT with a 100 µm spot size (200 mJ/cm^2 per pulse). We observed the discrete selective destruction of RPE after 6 hours without damage of underlying RPE basal lamina and extracellular matrix (**b**). Damage of cell membranes might be the effect of SRT induced microbubbles after SRT (**c**). Apical microvilli are absent after SRT compared with untreated cells (**a**).
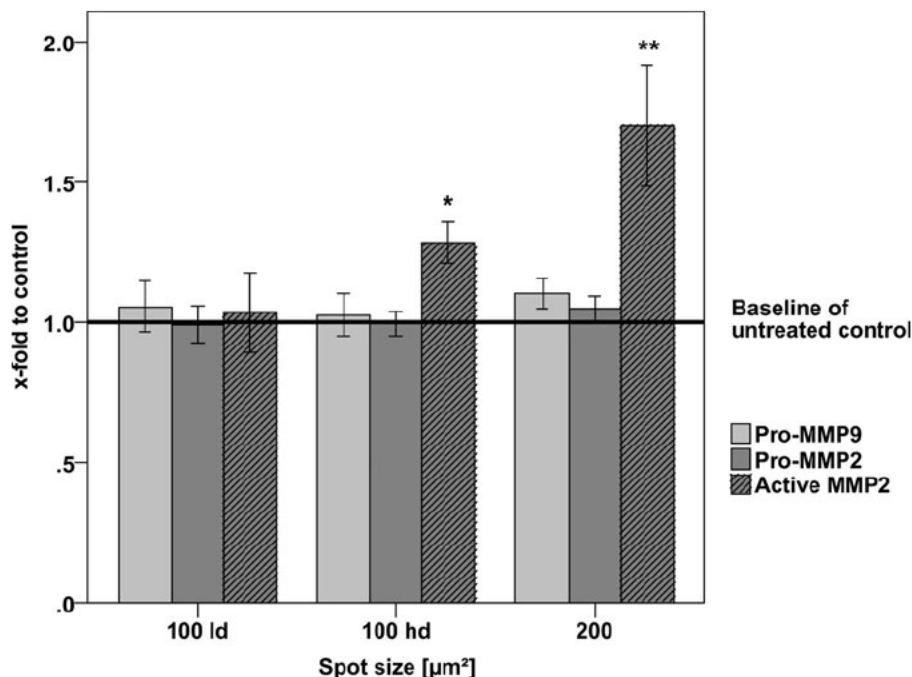
FIGURE 7. Secretion of MMPs after SRT using different spot sizes and densities. RPE choroid explants were irradiated with radiant exposures, which resulted in lesions above the threshold of cell death or cultivated as untreated controls. The content of different MMPs in culture medium of modified Ussing chambers is shown as fold of untreated controls (mean ± SEM). At day 4 after SRT, MMP level of ld treatment (100 μm spot size, 200 mJ/cm^2 per pulse) were not altered, even though the cumulative treated area was the same as in treatment with 200 μm spot size. In contrast, hd treatment with 100 μm spot size showed a moderate but significant increase of active MMP2 after 4 days, while pro MMP9 and pro MMP2 were not altered. After SRT with 200 μm spot size (140 mJ/cm^2 per pulse) the active form of MMP2 increased clear and significant related to control at day 4. This indicates that MMP release depends on spot size with an upregulation by the number of laser lesions. (*$P < 0.05$, **$P < 0.01$).

MMP2 levels showed no difference to control. Active MMP2 increased significantly after 4 days of cultivation to 1.75 fold ($P < 0.01$; Fig. 7).

Detection of MMP2 Expression by Immunofluorescence

The localization of SRT induced MMP2 expression after SRT with 200 μm spots was detected by immunofluorescence using RPE choroid flat mounts. The irradiated explants showed a localized expression of MMP2 in cell nuclei within the healing lesions while the surrounding cells showed no positive signal for MMP2 (Fig. 8).

Secretion of VEGF$_{165}$ After SRT

At day 4 the basolateral release of VEGF of explants, which were treated with a ld of small 100 μm spot, was not altered in comparison to untreated control. In the hd group with 100 μm spots, we observed a moderate but significant VEGF decrease to 0.91 fold ($P < 0.05$). The content of irradiated explants with 200 μm spot size decreased significantly after 4 days to 0.88 fold ($P < 0.05$) in comparison to untreated control (Fig. 9).

Influence of SRT on PEDF Secretion

PEDF levels showed no difference, neither in explants with 100 μm ld treatment nor in 100 μm hd treatment, compared with control. In contrast, the amount of PEDF increased significantly to 1.25 fold ($P < 0.05$) after 4 days in the choroid facing compartments of explants treated with 200 μm spots (Fig. 10).

DISCUSSION

Regeneration and Threshold Titration of RPE Cells

To minimize unspecific variability in cytokine release we chose a maximum observation time of 4 days, also referring to the transient effect of cellular dynamics after SRT as Treumer et al.[39] have shown. A maximum spontaneous cell death of 10% of the RPE cells in calcein staining was considered acceptable. The increase of cell size, appearance of prominent nuclei, presence of two nuclei in some RPE cells and the positive signal of mitosis marker Ki 67 after SRT indicate RPE migration and mitosis as part of PER, and therefore possible rejuvenation has also been demonstrated by others.[39,46] Four days after SRT, cell count analysis showed 53% recovering RPE cells in the irradiated area, compared with baseline (100%) of untreated RPE. We assume that a longer period of observation would show a further increase of cell number in the irradiated area. Differences in threshold of cell death between laser spots with 100 and 200 μm spot size were observed in this study, although unexpected compared with further studies.[38] Individual differences in pigmentation of porcine explants, which could influence the formation of microbubbles and cell disruption as well as variation in pulse durations between different energies, which were used for cultivation experiments, might be reasons for differences in threshold of SRT induced cell death between different spot sizes.

Release of Cell Mediators After SRT

The exchange of nutrients and waste products through BrM plays an important role in maintenance of the neuroretina. In AMD, the BrM is thickened and the supply of the neuroretina is
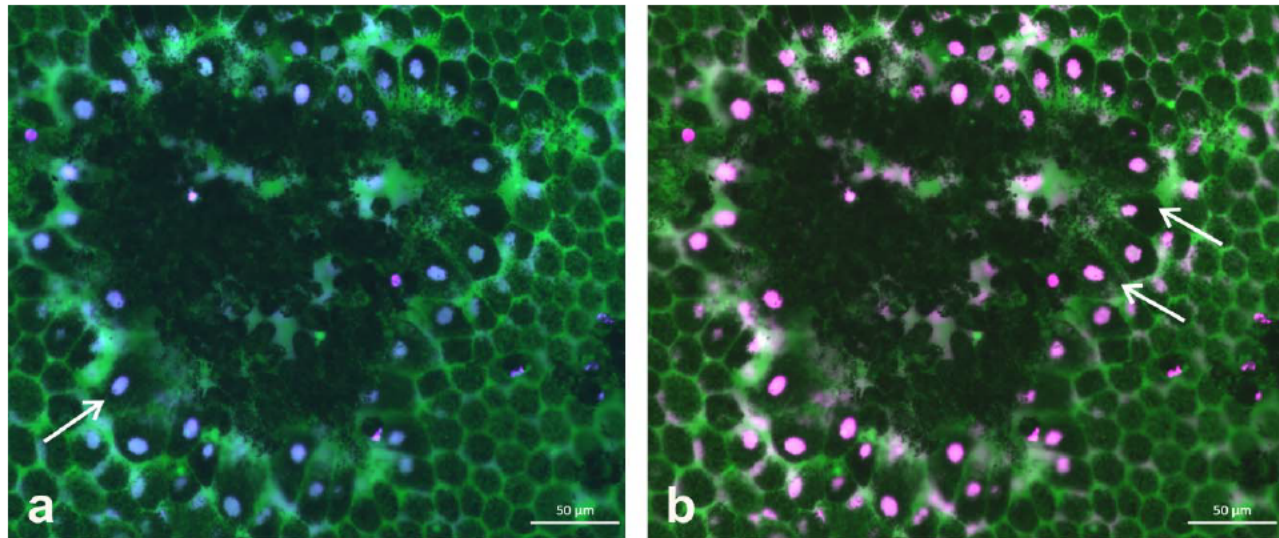
FIGURE 8. Immunofluorescence staining of MMP2 expression at RPE choroid explants. At day 3 of RPE regeneration F Actin was stained with phalloidin (*green*), cell nuclei with Hoechst (*blue, arrow* 5a) and MMP2 with Alexa fluor647. In immunofluorescence we observed a localized expression of MMP2 (*purple*) in cell nuclei (5b, *arrows*) of cells, which covered the SRT lesion after treatment with 200 μm spot size and radiant exposure of 140 mJ/cm^2 per pulse. Untreated RPE showed no positive signal for MMP2 in nuclei but sporadically at cell membranes. Magnification ×20.

reduced, which represents an important factor in development of multifactorial AMD. Therefore, we focused in this study on the basolateral release of AMD relevant cell mediators during PER to identify the SRT effect on the BrM facing site. AMD relevant mediators include MMPs with influence of BrM remodeling as well as VEGF and PEDF due to their pro and antiangiogenic properties.

Previous studies demonstrated that treatment of human BrM with activated MMPs leads to an enhancement of transport capacity.[19] In our study SRT treatment with 200 and 100 μm (only hd treatment) spots resulted in a basolateral

FIGURE 9. VEGF secretion of RPE choroid organ culture after SRT using different laser spot sizes. Explants were irradiated with radiant exposures, which resulted in lesions above the threshold of cell death or cultivated as untreated controls. The content of VEGF in basolateral culture medium of modified Ussing chambers is shown as fold of untreated controls (mean ± SEM). At day 4 after SRT, VEGF content of ld treatment with 100 μm spots (200 mJ/cm^2 per pulse) was not altered, but hd treatment with 100 μm lesions showed a moderate but significant reduction of VEGF. After SRT with 200 μm lesions (140 mJ/cm^2 per pulse) the VEGF content decreased clearly and significantly related to control. This indicates a lesion size and density dependent secretion of VEGF after SRT (*$P < 0.5$).

increase of active MMP2. This might lead to a reduction of a thickened BrM, which might improve the flux across the BrM to slow down or prevent the progression of early AMD.

The observed increase of active MMP2 was not an effect of cell death, but part of the regeneration process. A cell death induced increase of MMPs would also affect pro MMP2 and MMP9. The influence of pulsed laser irradiation on, for example, choroidal endothelial cells could not be tested separately in our system, while endothelial cells would also secrete cell mediators into basal compartments of modified Ussing chambers, like RPE cells do. In accordance with Treumer et al.,[39] we consider choroidal endothelial cells as a source for MMP release as unlikely, because Ahir et al.[19] have not observed the release of MMPs in human BrM choroid explants.

In this study, the content of pro MMP9 was not affected by SRT and active MMP9 was not detectable. Ahir et al.[19] have shown a cell cycle dependent release of active MMP9 in RPE cell cultures up to 24 hours after subcultivation. In this synchronized system, active MMP 9 release was terminated at half confluence of proliferating RPE. This suggests that MMP9 activation is taking place in a very early stage of cell proliferation and could explain the absence of active MMP9 in our study as analysis were performed at day 4, when the RPE layer was nearly restored. However, an excessive expression of active MMP9 may contribute to the development of CNV.[47–49]

The balance between the expression of proangiogenic cell mediators, such as VEGF and antiangiogenic cell mediators is highly regulated in the choroid RPE retina complex. A dysfunction of this balance is a crucial factor in the progression of AMD.[20] For prevention of AMD development as well as progression of dry AMD into wet AMD, a therapy with a moderate influence on pro and antiangiogenic cytokines is needed to generate a protein profile with nonneovascular properties.

The results of our study showed an increase of antiangiogenic PEDF and a decrease of proangiogenic VEGF following SRT treatment, corresponding to the indirect antiangiogenic effect of MMP2. This suggests that SRT may reduce the VEGF/ PEDF ratio and generate an antiangiogenic cytokine profile.
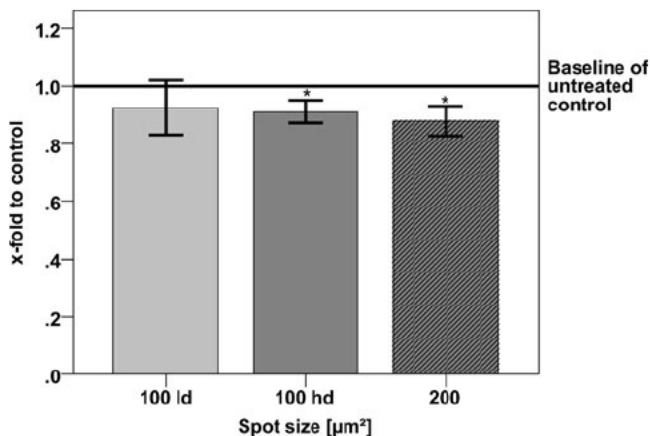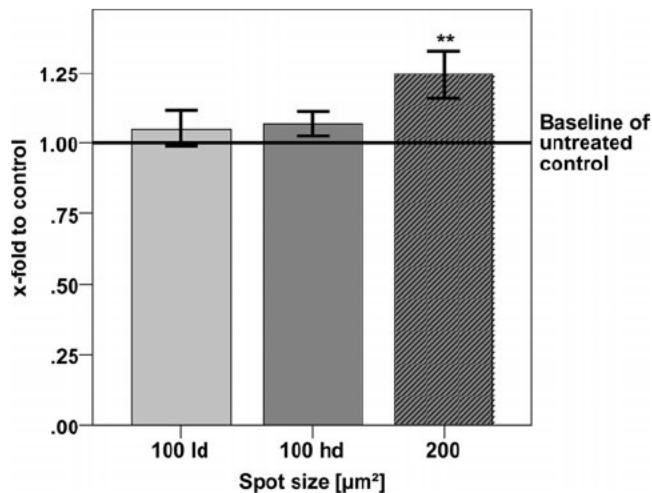
Figure 10. PEDF secretion of RPE choroid explants after SRT using different laser spot sizes. Explants were irradiated with radiant exposures, which resulted in lesions above the threshold of cell death or cultivated as untreated controls. Basolateral PEDF content in culture medium of modified Ussing chambers is shown as fold of untreated controls (mean ± SEM). PEDF secretion of ld as well as PEDF content of hd treatment group with 100 µm spots (200 mJ/cm^2 per pulse) was not affected after 4 days of cultivation. After SRT with 200 µm spot size (140 mJ/cm^2 per pulse) PEDF secretion increased significantly in comparison to control. This indicates a density and lesion size dependent secretion of PEDF after SRT (**$P < 0.01$).

Influence of Varying Spot Sizes and Densities

The pathology in AMD is limited to the macular region, and a SRT treatment with small spot sizes would enable a precise and safe treatment close to the fovea. The SRT had no effect on cytokines after ld treatment with small 100 µm spots, a moderate effect after hd treatment with 100 µm spots and a clear effect after treatment with large 200 µm spots. This indicates that SRT laser spot size and the density of lesions play an important role in secretion of cell mediators, which is an important finding for further in vivo studies.

CONCLUSIONS

We found an increase in the basolateral release of MMPs triggered by SRT dependent on spot size and density. This could lead to a reduction of a thickened BrM, and thereby improve the flux across BrM and reverse age related changes of BrM. The VEGF secretion was decreased and antagonistic PEDF secretion was increased by SRT. This could possibly prevent pathologic angiogenesis, such as CNV development. The SRT induced cytokine milieu might lead to a rejuvenation of the RPE BrM complex, and therefore represents a possible treatment for early AMD.

References

1. Schrader WF. Age related macular degeneration: a socioeconomic time bomb in our aging society [in German]. *Ophthalmologe*. 2006;103:742 748.
2. Green WR. Histopathology of age related macular degeneration. *Mol Vis*. 1999;5:27.
3. Parmeggiani F, Sorrentino FS, Romano MR, et al. Mechanism of inflammation in age related macular degeneration: an up to date on genetic landmarks. *Mediators Inflamm*. 2013;2013: e435607
4. Sarks S, Cherepanoff S, Killingsworth M, Sarks J. Relationship of basal laminar deposit and membranous debris to the clinical presentation of early age related macular degeneration. *Invest Opthalmol Vis Sci*. 2007;48:968 977.
5. Hampton BM, Kovach JL, Schwartz SG. Pharmacogenetics and nutritional supplementation in age related macular degeneration. *Clin Ophthalmol*. 2015;9:873 876.
6. Hillenkamp J, Hussain AA, Jackson TL, Cunningham JR, Marshall J. The influence of path length and matrix components on ageing characteristics of transport between the choroid and the outer retina. *Invest Ophthalmol Vis Sci*. 2004;45:1493 1498.
7. Hussain AA, Starita C, Hodgetts A, Marshall J. Macromolecular diffusion characteristics of ageing human Bruch's membrane: implications for age related macular degeneration (AMD). *Exp Eye Res*. 2010;90:703 710.
8. Moore DJ, Clover GM. The effect of age on the macromolecular permeability of human Bruch's membrane. *Invest Ophthalmol Vis Sci*. 2001;42:2970 2975.
9. Curcio CA, Millican CL, Bailey T, Kruth HS. Accumulation of cholesterol with age in human Bruch's membrane. *Invest Ophthalmol Vis Sci*. 2001;42:265 274.
10. Handa JT, Verzijl N, Matsunaga H, et al. Increase in the advanced glycation end product pentosidine in Bruch's membrane with age. *Invest Ophthalmol Vis Sci*. 1999;40: 775 779.
11. Karwatowski WS, Jeffries TE, Duance VC, Albon J, Bailey AJ, Easty DL. Preparation of Bruch's membrane and analysis of the age related changes in the structural collagens. *Br J Ophthalmol*. 1995;79:944 952.
12. Okubo A, Rosa RH, Bunce CV, et al. The relationships of age changes in retinal pigment epithelium and Bruch's membrane. *Invest Ophthalmol Vis Sci*. 1999;40:443 449.
13. Sternlicht MD, Werb Z. How matrix metalloproteinases regulate cell behavior. *Annu Rev Cell Dev Biol*. 2001;17: 463 516.
14. Alexander JP, Bradley JM, Gabourel JD, Acott TS. Expression of matrix metalloproteinases and inhibitor by human retinal pigment epithelium. *Invest Ophthalmol Vis Sci*. 1990;31: 2520 2528.
15. Guo L, Hussain AA, Limb GA, Marshall J. Age dependent variation in metalloproteinase activity of isolated human Bruch's membrane and choroid. *Invest Ophthalmol Vis Sci*. 1999;40:2676 2682.
16. Padgett LC, Lui GM, Werb Z, Lavail MM. Matrix metalloproteinase 2 and tissue inhibitor of metalloproteinase 1 in the retinal pigment epithelium and interphotoreceptor matrix: vectorial secretion and regulation. *Exp Eye Res*. 1997;64:927 938.
17. Vranka JA, Johnson E, Zhu X, et al. Discrete expression and distribution pattern of TIMP 3 in the human retina and choroid. *Curr Eye Res*. 1997;16:102 110.
18. Hussain AA, Lee Y, Zhang JJ, Marshall J. Disturbed matrix metalloproteinase activity of Bruch's membrane in age related macular degeneration. *Invest Ophthalmol Vis Sci*. 2011;52: 4459 4466.

19. Ahir A, Guo L, Hussain AA, Marshall J. Expression of metalloproteinases from human retinal pigment epithelial cells and their effects on the hydraulic conductivity of Bruch's membrane. *Invest Ophthalmol Vis Sci*. 2002;43:458 465.

20. Ohno Matsui K, Morita I, Tombran Tink J, et al. Novel mechanism for age related macular degeneration: an equilib rium shift between the angiogenesis factors VEGF and PEDF. *J Cell Physiol*. 2001;189:323 333.

21. Kwak N, Okamoto N, Wood JM, Campochiaro PA. VEGF is major stimulator in model of choroidal neovascularization. *Invest Ophthalmol Vis Sci*. 2000;41:3158 3164.

22. Blaauwgeers HG, Holtkamp GM, Rutten H, et al. Polarized vascular endothelial growth factor secretion by human retinal pigment epithelium and localization of vascular endothelial growth factor receptors on the inner choriocapillaris. Evidence for a trophic paracrine relation. *Am J Pathol*. 1999;155:421 428.

23. Bouck N. PEDF: anti angiogenic guardian of ocular function. *Trends Mol Med*. 2002;8:330 334.

24. Cao W, Tombran Tink J, Elias R, Sezate S, Mrazek D, McGinnis JF. In vivo protection of photoreceptors from light damage by pigment epithelium derived factor. *Invest Ophthalmol Vis Sci*. 2001;42:1646 1652.

25. Dawson DW, Volpert OV, Gillis P, et al. Pigment epithelium derived factor: a potent inhibitor of angiogenesis. *Science*. 1999;285:245 248.

26. Jablonski MM, Tombran Tink J, Mrazek DA, Iannaccone A. Pigment epithelium derived factor supports normal develop ment of photoreceptor neurons and opsin expression after retinal pigment epithelium removal. *J Neurosci*. 2000;20: 7149 7157.

27. Mori K, Gehlbach P, Yamamoto S, et al. AAV mediated gene transfer of pigment epithelium derived factor inhibits choroi dal neovascularization. *Invest Ophthalmol Vis Sci*. 2002;43: 1994 2000.

28. Figueroa MS, Regueras A, Bertrand J. Laser photocoagulation to treat macular soft drusen in age related macular degener ation. *Retina (Philadelphia, Pa)*. 1994;14:391 396.

29. Ho AC, Maguire MG, Yoken J, et al.; for the Choroidal Neovascularization Prevention Trial Research Group. Laser induced drusen reduction improves visual function at 1 year. *Ophthalmology*. 1999;106:1367 1373; discussion 1374.

30. Roider J, Michaud N, Flotte T, Birngruber R. Histology of retinal lesions after continuous irradiation and selective micro coagulation of the retinal pigment epithelium [in German]. *Ophthalmologe*. 1993;90:274 278.

31. Rodanant N, Friberg TR, Cheng L, et al. Predictors of drusen reduction after subthreshold infrared (810 nm) diode laser macular grid photocoagulation for nonexudative age related macular degeneration. *Am J Ophthalmol*. 2002;134:577 585.

32. Friberg TR, Brennen PM, Freeman WR, Musch DC; for the PTAMD Study Group. Prophylactic treatment of age related macular degeneration report number 2: 810 nanometer laser to eyes with drusen: bilaterally eligible patients. *Ophthalmic Surg Lasers Imaging*. 2009;40:530 538.

33. Owens SL, Bunce C, Brannon AJ, et al. Prophylactic laser treatment hastens choroidal neovascularization in unilateral age related maculopathy: final results of the drusen laser study. *Am J Ophthalmol*. 2006;141:276 281.

34. Brinkmann R, Roider J, Birngruber R. Selective retina therapy (SRT): a review on methods, techniques, preclinical and first clinical results. *Bull Soc Belge Ophtalmol*. 2006;(302):51 69.

35. Roider J, Michaud NA, Flotte TJ, Birngruber R. Response of the retinal pigment epithelium to selective photocoagulation. *Arch Ophthalmol*. 1992;110:1786 1792.

36. Roider J, El Hifnawi ES, Birngruber R. Bubble formation as primary interaction mechanism in retinal laser exposure with 200 ns laser pulses. *Lasers Surg Med*. 1998;22:240 248.

37. Roider J, Brinkmann R, Wirbelauer C, Laqua H, Birngruber R. Retinal sparing by selective retinal pigment epithelial photocoagulation. *Arch Ophthalmol*. 1999;117:1028 1034.

38. Brinkmann R, Huttmann G, Rogener J, Roider J, Birngruber R, Lin CP. Origin of retinal pigment epithelium cell damage by pulsed laser irradiance in the nanosecond to microsecond time regimen. *Lasers Surg Med*. 2000;27:451 464.

39. Treumer F, Klettner A, Baltz J, et al. Vectorial release of matrix metalloproteinases (MMPs) from porcine RPE choroid ex plants following selective retina therapy (SRT): toward slowing the macular ageing process. *Exp Eye Res*. 2012;97: 63 72.

40. Zhang JJ, Sun Y, Hussain AA, Marshall J. Laser mediated activation of human retinal pigment epithelial cells and concomitant release of matrix metalloproteinases laser activation of human RPEs and MMP release. *Invest Ophthal mol Vis Sci*. 2012;53:2928 2937.

41. Roider J, Brinkmann R, Wirbelauer C, Laqua H, Birngruber R. Subthreshold (retinal pigment epithelium) photocoagulation in macular diseases: a pilot study. *Br J Ophthalmol*. 2000;84: 40 47.

42. Framme C, Brinkmann R, Birngruber R, Roider J. Autofluo rescence imaging after selective RPE laser treatment in macular diseases and clinical outcome: a pilot study. *Br J Ophthalmol*. 2002;86:1099 1106.

43. Elsner H, Porksen E, Klatt C, et al. Selective retina therapy in patients with central serous chorioretinopathy. *Graefes Arch Clin Exp Ophthalmol*. 2006;244:1638 1645.

44. Elsner H, Klatt C, Liew SHM, et al. Selective retina therapy in patients with diabetic maculopathy [in German]. *Ophthalmo loge*. 2006;103:856 860.

45. Klettner A, Roider J. Comparison of bevacizumab, ranibizu mab, and pegaptanib in vitro: efficiency and possible additional pathways. *Invest Ophthalmol Vis Sci*. 2008;49: 4523 4527.

46. Flaxel C, Bradle J, Acott T, Samples JR. Retinal pigment epithelium produces matrix metalloproteinases after laser treatment. *Retina (Philadelphia, Pa)*. 2007;27:629 634.

47. Lambert V, Munaut C, Jost M, et al. Matrix metalloproteinase 9 contributes to choroidal neovascularization. *Am J Pathol*. 2002;161:1247 1253.

48. Bergers G, Brekken R, McMahon G, et al. Matrix metal loproteinase 9 triggers the angiogenic switch during carcino genesis. *Nat Cell Biol*. 2000;2:737 744.

49. Hollborn M, Stathopoulos C, Steffen A, Wiedemann P, Kohen L, Bringmann A. Positive feedback regulation between MMP 9 and VEGF in human RPE cells. *Invest Ophthalmol Vis Sci*. 2007;48:4360 4367.